19th Brazilian Congress of Thermal Sciences and Engineering
November 6th–10th, 2022, Bento Gonçalves - RS - Brazil

ENC-2022-0716
THERMAL MODELS OF DIRECT MOLTEN SALT LINEAR FRESNEL SYSTEM

Vinicius Rugeri Borges Bonini
vinicius.bonini@lepten.ufsc.br
Allan Ricardo Starke
allan.starke@lepten.ufsc.br
Alexandre Kupka da Silva
a.kupka@ufsc.br
Laboratory of Energy Conversion Engineering and Energy Technology - Technological Center - Federal University of Santa Catarina - LEPTEN/CTC/UFSC.
Trindade, Florianópolis, SC, CEP 88040-900, Brazil.

Abstract. *Renewable energy sources are essential in reducing our global dependence on fossil fuels. Among the renewable sources, solar energy has high potential, mainly because it allows a decentralized installation and because of the variety of technologies and applications available. Linear Fresnel Collector (LFC) system presents itself as an option, mainly due to its simplicity. Linear Fresnel plants generally operate in one of two different schemes: (i) direct steam generation (DSG), where water is used as the HTF and it is directly converted to steam, and (ii) direct molten salt (DMS), where molten salt is used as HTF. In the latter, water vapor can be produced by within heat exchanger that uses molten salt as hot fluid. Due to its relatively short existence, detailed thermal models of LFC plants operating with molten salts as a heat transfer fluid are not widely available. In this sense, the development of a reliable mathematical model that allows designers to predict and optimize its performance is fundamental to the proliferation of this technology. Therefore, the present work will propose a transient thermal mathematical model for the linear Fresnel system with molten salt as heat transfer fluid, and additionally, assess the main parameters that most influences its behavior.*

Keywords: *Linear fresnel collectors, molten salts, transient simulation, thermal model.*

1. INTRODUCTION

Humankind requires energy for improving the quality of live, both for the basic energy needs, and to supply production processes and economic growth. Estimates suggest a 40% increase in the global energy demand from primary sources until 2040 (OPEC, 2016). In 2019, the world demand for primary energy was $602.27\ EJ$, of which, 31% ($188.91\ EJ$) were met through oil, 26% ($157.51\ EJ$) were met by coal, and 23% ($139,\ 00\ EJ$) were supplied by natural gas(IEA, 2019). As for renewable sources, these represented 14% of the energy production matrix in 2019, indicating a growth of 12.2% between 2018 and 2019 (IEA, 2019). Therefore, the question that should be answered is how do we meet these energy requirements without compromising the well-being of our future generations?

Solar energy is one of the renewable sources with greater potential to reduce dependence on fossil fuels, being able to satisfactorily meet thermal (SPF, 2017) and electrical (Zurita *et al.*, 2020; Wagner *et al.*, 2017; Starke *et al.*, 2016) demands. The generation of electrical energy can be carried out directly through photovoltaic cells (PV), or through thermal cycles in solar concentration plants (CSP[1]). Both technologies have shown growth in the number of projects in recent years, causing a reduction in the Levelized Cost of Energy (LCOE) (Colla *et al.*, 2020), reaching economically competitive values with fossil fuels (IRENA, 2018). Regarding CSP plants, there was a significant reduction in costs between 2010 and 2018, with an average LCOE of around $0.185\ USD2018/kWh$(IRENA, 2018).

The presence of energy storage allows the system to be able to generate electric energy in a constant way, in addition, the electric energy dispatch can be optimized so that the electric energy is produced in periods of higher tariff, or of greater demand, reducing the need for non-renewable sources (Zurita *et al.*, 2020; Wagner, 2017; Hamilton *et al.*, 2020; Vasallo and Bravo, 2016). Therefore, to have a flexible electricity production, an energy reservoir is necessary. For CSP plants, a thermal energy storage (TES) is used since it can be easily associated with steam thermal cycles (Rankine cycle)

[1]Concentrated solar power

adopted to convert thermal energy to electricity. On the other hand, PV systems use batteries as energy reservoir. Thermal energy storage is cheaper when compared to electrical energy storage in batteries, being more viable for large electricity generation projects (Gallego *et al.*, 2020).

There are four main technologies for concentrating solar collectors. The first set is the linear focus systems, composed of parabolic cylindrical collectors (PTC[2]) and linear Fresnel collectors (LFC[3]). The second group refers to systems with point focus, such as the central receiver (CRS[4]) and parabolic disks. More specifically, Linear Fresnel technology consists of a set of mirrors arranged in lines, each with uni-axial tracking and located close to the ground, and which are responsible for reflecting solar radiation and concentrating it in an absorber tube located above, the mirrors. One can argue that Linear Fresnel Collector is a simplified concept of the well know parabolic trough collectors, which adopts a different design for the concentrating mirrors, replacing the parabolic mirror with a set of flat (or slightly curved) one-tracking mirrors. This set of mirrors reflects the solar irradiation to a fixed receiver, positioned above of the mirrors, with their absorbing tube facing downwards Zhu *et al.* (2014); Vouros *et al.* (2020). The receiver is composed of metallic tubes with selective coating through which the heat transfer fluid (HTF) flows. Some receivers uses a second reflector above the receiver, which corrects the focal line of the irradiation reflected in the primary reflectors Gazzo *et al.* (2011). Theses tubes can be inside an evacuated glass envelop or simply inside a cavity sealed by a glass plate.

Two different operational schemes are mainly used in LFC plants, depending of which HTF is used to absorb the solar energy: direct molten salt (DMS) uses molten salts or direct steam generation (DSG) uses water being directly vaporized in the absorber tubes. DMS scheme can be directly coupled with molten salt TES, without the need of a heat exchanger between the solar field and TES system. While, the DSG schemes can be directly coupled with the power block, without requiring a heat recovery steam generator to generate the steam used in the Rankine cycle from the HTF.

The constructive simplicity of the LFC system is its biggest advantage over other CSP technologies. The use of small flat (or slightly curved) mirrors results in lower initial investment, due to the lower equipment and construction cost. While the use of fixed absorber tubes eliminate the need of rotary joints required in the PTC plants to allow the absorber to move at the focal point, which results in lower investment and maintenance cost. However, simplifying the mirror geometry generates a disadvantage for the LFC, a lower concentrating ratio and optical efficiency. Therefore, the theoretical maximum HTF temperature will be lower, resulting in a lower efficiency of the power block, and a lower efficiency in the conversion of solar irradiation into heat, both reducing the overall efficiency of the plant.

Regarding the type of salt used, in general, salts composed of nitrates are more used in solar applications, given their low cost and favorable properties. Among them, the reduced corrosion with typical pipe materials, thermal stability at high temperatures and low environmental impact stand out. Furthermore, because there is no phase shift, the controllability of the system is simplified compared to the two-phase flow of the DSG mode. On the other hand, binary (Solar Salt) and ternary (HITEC and HITEC-XL) molten salts have a high freezing point in the range of $120 - 220°C$, which requires systems that prevent the solidification of salts in pipes and tanks (e.g. heat trace) (Hakkarainen and Tähtinen, 2016; Benoit *et al.*, 2016).

Recent works on LFC have focused on improving the thermal and optical performance of this technology (Tsekouras *et al.*, 2018; Bellos *et al.*, 2018, 2019; Vouros *et al.*, 2019, 2020), as well as its control system (Gallego *et al.*, 2020). Another topic refers to the thermal fluid used, which will allow the LFC system to reach higher operating temperatures (Bachelier and Jäger, 2019). LFC-DMS plants have been studied by several authors (Grena and Tarquini, 2011; Schneider *et al.*, 2015; Bachelier and Stieglitz, 2017), who, in general, state that the DMS concept currently represents the most promising technological option, in terms of LCOE optimization, for plants with thermal energy storage.

Wherefore, the present work focus on the mathematical modelling of a LFC-DMS collector power plant, searching to reproduce the real thermal behavior of the system, employing an accepted software as reference. After that, some operational aspects of the plant's operation will be investigated, searching to verify the benefits of the LFC-DMS technology. The TRNSYS©(Klein, 2010) software will be use to assess the transient performance of the LFC-DMS plant.

2. MATHEMATICAL MODEL DESCRIPTION

The mathematical models of the DMS-LFC plant is based in the SAM© physical trough model (Wagner and Gilman, 2010), which was modified to account the optical characteristics of the Fresnel collector.

2.1 Solar Field

The solar field is composed by N_{loops} identical loops disposed in parallel. Each loop is composed by multiple modules, called solar collector assembly (SCA), which are not necessarily identical. Several identical collectors installed in series will generate a SCA. SCA's installed in series - that could be from different manufactures - will produce a loop.

Each SCA considers the mirrors - optical model - and the heat collection element (HCE) - thermal model of the

[2]Parabolic Trough Collectors
[3]Linear Fresnel Collectors
[4]Central Receiver System

absorber pipes. Since N_{SCA} are considered in series, the model considers the N_{SCA} as an axial discretization of the loop, accounting for the increase of the HTF temperature over the length of the loop.

A header pipe feeds each field loop with the HTF mass flow rate ($\dot{m}_{HTF}$), while a second header pipe collects the heated HTF and directs it to the thermal storage or the power block. These header pipes should be designed to guarantee a balanced flow in each loop. Thus, the solar field can be modeled as identical loops required to simulate the thermal-hydraulic performance of one collector loop, which is then multiplied by N_{loops} to calculate the yield of the entire field.

The optical and thermal-hydraulic models of the SCA and the thermal-hydraulic of the header pipes are described as follows. The optical model accounts for the optical inefficiencies of the solar irradiation from the mirrors to the receiver. Thus, the incident irradiation in the HCE is calculated as follows,

$$\dot{q}_{inc,HCE} = DNIA_{aperture,SCA}\eta_{optical}, \tag{1}$$

where $\eta_{optical}$ is the optical efficiency of the SCA for any particular time of the day, therefore, accounting for the effects of the incident angle. Calculating the optical efficiency considering all the geometrical aspects of the Fresnel Collector is not a simple task, requiring a ray-tracing analysis to consider the bi-directional nature of the reflection, this being infeasible in transient simulation. The solution is to use Incident Angle Modifiers (IAM) data or correlations to account for the non-normal incidence. IAM data are provided by the manufactures of the solar collector through experiments as a function of the collector incident angles. In this sense, the SCA optical efficiency is calculated as,

$$\eta_{optical} = \eta_{SCA,n} IAM_{avg} f_t, \tag{2}$$

where $\eta_{SCA,n}$ is the global optical efficiency at normal incidence of irradiation, which can be calculated multiplying the efficiencies of the different phenomena in the collector, i.e. $\eta_{tracking}$, η_{Geom}, $\eta_{rho,mirror}$, η_{dirt}, η_{error}, related to a fixed optical loss representing collector tracking error, a fixed optical loss representing the collector's geometry effects, the optical loss fraction associated with mirror reflectivity, the optical loss fraction associated with soiling on the mirrors and any other optical loss not captured in the IAM. These parameters are provided by the manufacture or should be defined by the user. IAM_{avg} is the Incident Angle Modifier calculated as a function of the longitudinal (θ_L) and transversal (θ_T) collector incident angles (Wagner and Gilman, 2010). The subscript *avg* is related to the average IAM for the simulation time-step being evaluated, usually calculated using the θ_L and θ_T evaluated in the middle of time interval. For example, between 10 to 11 am (Solar time), the $IAM_{avg} \approx IAM(\theta_L(10.5h), \theta_T(10.5))$. Finally, f_t is a tracking parameter that accounts for the fraction of the time-step that the solar collector was effectively tracking the sun. It is an important parameter during sunrise and sunset that helps to consider the deployment and stow angles.

The thermal-hydraulic model of the solar field calculates the mass flow rate of the HTF that the field can provide at a desired design temperature and at a specific time of the day, i.e. at a specific DNI and incident angle; and the related pressure drop across the field.

The thermal model solves the energy equation of the collector loop and the two headers pipe (cold header delivers mass flow to the loops and the hot header collects the heated mass flow). In combination with a hybrid iteration method (Wagner and Gilman, 2010), the models are implemented in a numerical scheme similar to a close loop controller, i.e. the HTF mass flow rate is modulated to guarantee a desired HTF temperature at the field outlet.

The temperatures of the cold and hot headers are calculated using the lumped capacity model, as follows (Wagner and Gilman, 2010),

$$\left[\bar{V}_c(\rho c)_{htf,c} + (mc)_c\right] \frac{dT_c}{dt} = \dot{m}_{htf} N_{loops} c_{htf,c}(T_{sf,in} - T_c), \tag{3}$$

$$\left[\bar{V}_h(\rho c)_{htf,h} + (mc)_h\right] \frac{dT_h}{dt} = \dot{m}_{htf} N_{loops} c_{htf,h}(T_{h,header,in} - T_h), \tag{4}$$

where $\bar{V}$ is the volume of the pipes, (mc) is the heat capacity of the pipes and accessories. c_{htf} and $\dot{m}_{htf}$ are the heat capacity and mass flow rate of the HTF in the loop. The temperatures T_h and T_c represent the mean temperature of the header pipes, while $T_{h,header,in}$ is the temperature of the HTF at the inlet of the hot header and $T_{sf,in}$ is the temperature of the HTF at the inlet of the cold header. The subscripts h and c are related to the hot and cold header.

Equations 3 and 4 are solved using the forward $(p+1)$ Euler method, therefore, the properties are evaluated at the known temperature (p), i.e. fully explicit method.

The inlet temperature of the loop is calculated accounting for the heat loss over the header pipe as follows,

$$T_{loop_in} = T_c - \dot{Q}_{loss,pipe,cold}/(\dot{m}_{htf} N_{loops} c_{htf,c}). \tag{5}$$

The inlet temperature of the hot header is calculated accounting for the heat loss over the header pipe as follows,

$$T_{h,header,in} = T_{loop_out} - \dot{Q}_{loss,pipe,hot}/(\dot{m}_{htf} N_{loops} c_{htf,h}), \tag{6}$$

where $\dot{Q}_{loss,pipe,cold}$ and $\dot{Q}_{loss,pipe,hot}$ are the thermal losses in the field pipes, calculated through Newton's law of cooling, considering an overall heat loss coefficient $(h_{loss,hdr})$, the tubes diameters (D) and lengths (L). The thermal loss considers the change in the diameter of the tubes as it collects/delivers flow from/to the multiple loops; a full description of the header design is presented in (Wagner and Gilman, 2010).

The thermal model of the HCE solves the energy equation of a control volume including the absorber pipe, as fully described by (Wagner and Gilman, 2010), thus,

$$\frac{\partial U}{\partial t} = \dot{q}_{in} - \dot{q}_{out} + \dot{q}_{abs} = \frac{\partial U}{\partial t} = \left((mc)_{HTF} + L_{SCA}\,(mc)_{HCE}\right)\frac{\partial \bar{T}}{\partial t} = \dot{m}_{HTF}\left(T_{in} - \bar{T_{out}}\right) + \dot{q}_{abs}, \tag{7}$$

where $\partial U/\partial t$ represents the rate of change in the internal energy of the HCE, considering the thermal capacity of the pipe $(mc)_{HCE}$ and HTF $(mc)_{HTF}$. $\bar{T}$ is the average temperature of the HCE. $\dot{q}_{in}$ represents the energy transported by advection in the control volume, while $\dot{q}_{out}$ represents the energy transported by advection out to the control volume. Therefore, $\dot{q}_{in} - \dot{q}_{out} = \dot{m}_{HTF} c_{HTF}(T_{in} - T_{out})$. Finally, $\dot{q}_{abs}$ represents the net power absorbed by the HCE and HTF, which can be calculated as follow,

$$\dot{q}_{abs} = \dot{q}_{inc,HCE} - \dot{q}_{loss,HCE}, \tag{8}$$

where $\dot{q}_{inc,HCE}$ is the incident radiation in the HCE, calculated by equation 1, while, $\dot{q}_{HCE,loss}$ represents the power loss of the absorber tube, that can be calculated by a correlation provided by the manufacturer or by a physical model. In this context, there are two options, using a polynomial model, or using the Forristall model (Forristall, 2003), a steady state radial heat transfer model for a evacuated tube, being the latter used in the present model. The Forristal models is fully described in (Forristall, 2003) and (Wagner and Gilman, 2010).

Equation 7 can be solved analytically if written in a more convenient form and some considerations are made. First, one must acknowledge that the average temperature of the HCE is $\bar{T} = \left(T_{in} - T_{out}\right)/2$, and then, $T_{out} = T_{in} - 2\bar{T}$, substituting this expression in Equation 7,

$$\frac{\partial \bar{T}}{\partial t} = \frac{2\dot{m}_{HTF}\left(T_{in} - \bar{T}\right)}{(mc)_{HTF} + (mc)_{HCE}} + \frac{\dot{q}_{abs}}{(mc)_{HTF} + (mc)_{HCE}}. \tag{9}$$

Considering the thermodynamic and transport properties as a constant, equation 9 is a non-homogeneous ordinary differential equation in the form $\frac{d\theta}{dt} + a\theta - b = 0$. With the transformation $\theta' = \theta - \frac{b}{a}$, therefore, the EDO can be written in a homogeneous form, $\frac{d\theta'}{dt} + a\theta' = 0$ and solved by separating the variables and integrating (Incropera *et al.*, 2007). Therefore, the outlet temperature of the HCE (T_{out}) is calculated as follows (Wagner and Gilman, 2010),

$$T_{out} = \frac{\dot{q}_{abs}}{(mc)_{HTF}} + T_{in} + 2\left(\bar{T_0} - \frac{\dot{q}_{abs}}{2(mc)_{HTF}} - T_{in}\right)\exp\left[\frac{-2(mc)_{HTF}\Delta t}{(mc)_{HTF} + (mc)_{HCE}}\right], \tag{10}$$

where $\bar{T_0}$ is the average temperature of the HCE in the previous time-step. This equation is applied for each of the SCA in a loop, considering T_{in} and the outlet temperature of the previous SCA. The non-linearity of the thermodinamic/transport properties and the net power absorbed by the HCE $\dot{q}_{abs}$ (Forristal model) are accounted through an iterative process used to solve the thermal resistance network of the Forristal model.

Regarding the hydraulic model, the pressure drop along the header pipes, collector loop and accessories are calculated using the Reynolds number and friction factor in order to determine the head loss and pressure difference. The friction is calculated using the Colebrook–White correlation (Colebrook, 1939). Calculating the total pressure drop across the field is a complex task since it requires a detailed design of all pipes and accessories. More details of the model can be found in (Wagner and Gilman, 2010).

2.2 Thermal Energy Storage, Plant Control and Power Block

The mathematical models used for the thermal energy storage, plant control and power block are identical to the one used in the parabolic trough plant developed by NREL (Wagner and Gilman, 2010; Wagner, 2017), and fully described by theses authors. Briefly, it is worth mentioned that a two tank, direct thermal energy system performance is simulated solving the First Law of thermodynamic for an open system. The ODE of the tank temperature as a function of time and can be solved analytically if the thermodynamic properties are evaluated at the average tank temperature of the previous time-step. The thermal losses can be calculated implicitly through the system of equations, or approximated using the average temperature of the tank in the current time step.

The controller uses a control tree do decide between the operation modes of the plant, i.e. start-up, operation below the minimum power block mass flow; part-load of the power block, between the minimal operation condition and nominal power production; over-design operation with more energy absorbed in the solar field than can be used by the power block

and/or storage, so defocusing of mirrors is required; and finally, over-design operation where all of the energy can be used in the power block and/or storage.

The power block model must consider the part load operation of the Rankine cycle, this is done using dimensionless performance curves developed by (Wagner, 2017), and validated using real data from SEGS plants. The cycle performance is assessed using curves for the heat power input ($\dot{Q}_{pb,in}$) and power output ($\dot{W}_{pb,gross}$) as a function of the inlet HTF temperature ($T_{HTF,pb,in}$), power block HTF mass flow rate ($\dot{m}_{HTF,pb}$) and condenser pressure p_c. The condenser pressure is calculated using a detailed performance model of a dry cooling system, also described by (Wagner and Gilman, 2010).

3. METHODS

To verify if the behavior of the implemented mathematical model in TRNSYS© is correct, a comparison was performed. For that purpose the Brazilian city of Bom Jesus da Lapa, was chosen once this city presents one of the best incident radiation in the whole brazilian territory. The city is located at latitude $-13.26°$, longitude -43.42 ° and $440m$ of altitude. The data was collected by INMET, with a design point DNI of 1000 W/m^2, a daily total for DNI of 2.65 kWh/m^2 and a daily total for DNI of 2.29 kWh/m^2.

Regarding the linear Fresnel plant, n usual layout was used, composed by the solar field, two thermal storages, three salt-water heat exchangers and a Rankine thermal cycle, as depicted in Figure 1. Concerning the LFC-DMS plant parameters, the default values from SAM© were used, which are: a solar multiple of 2.3, a field aperture area of $1.12872e^6m^2$, an irradiation at design of 950 W/m^2, with 16 collectors per loop with 150 loops and a design inlet temperature of $295°C$. The optical characterization of the collector is through the IAM[5] table and the receiver heat losses are modeled with the evacuated tube model.

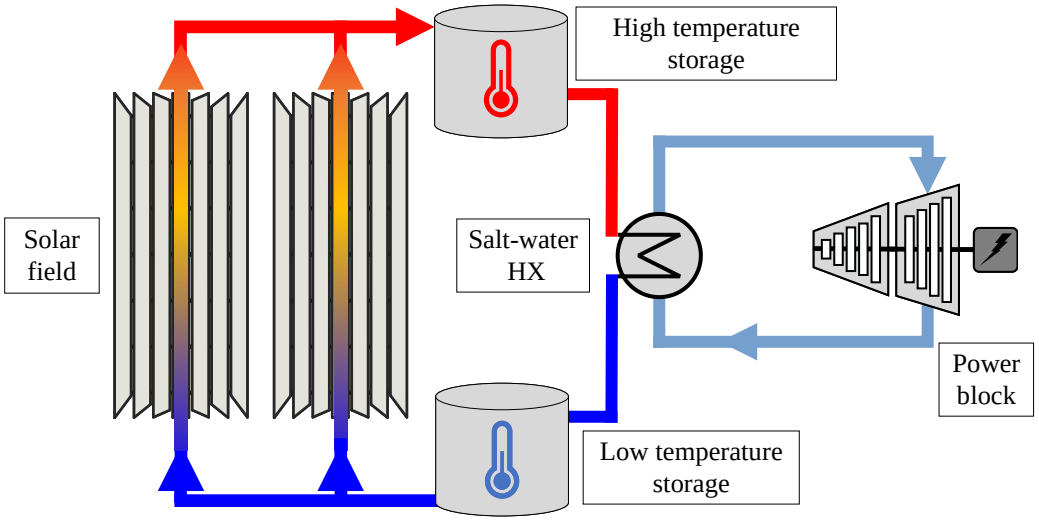

Figure 1. Simplified diagram of the LFC-DMS power plant with two thermal storages.

The HTF and storage media is Solar Salt[6] with an equivalent capacity of 4 $hours$, which corresponds to a thermal capacity of 1119.51 MW and a total volume of 6273.08 m^3. Concerning the power cycle, the nominal power is 111.11 MW, gross power to net power efficiency of 90%, thermal cycle conversion efficiency of 39.7%, inlet temperature of $525°C$ and pressure of 100 bar, with a fixed pressure control to the inlet pressure and to the condenser air-cooled.

4. RESULTS AND DISCUSSION

The capacity of the implemented tool to properly reproduce the thermal/hydraulic behavior of the LFC-DMS system is imperative. In this context, it is important to point out that, for the electricity generation through thermal cycles (Rankine in this case), the inlet temperature is fixed, therefor, the mass flow rate of the solar field must be adjusted to match the temperature. A comparison for the flow rate in the solar field is presented in Figure 2, where, the blue line represents the TRNSYS© result, the orange line represents SAM© and the black dots concerns the normalized relative difference between SAM© and TRNSYS©.

[5] Incidence angle modifier
[6] 60%$NaNO_3$+40% KNO_3

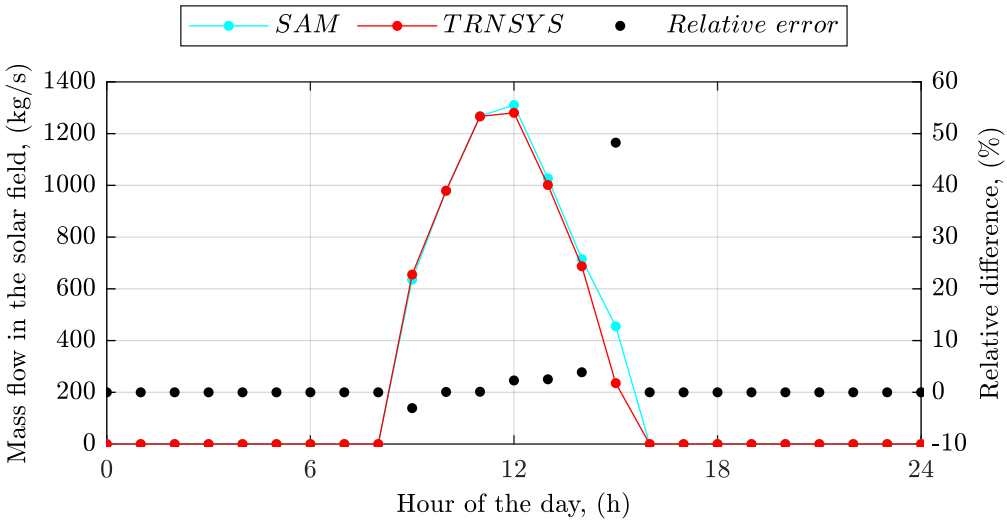

Figure 2. Field flow comparison of collectors, for TRNSYS© and SAM©.

The period selected comprehends to one day of operation of the solar field. It remains clear that there are small differences in the later hours of the day, namely, SAM© operates one more hour in comparison to the TRNSYS© operation, while TRNSYS© starts with a larger flow rate in the solar field. This difference is possibly caused by control parameters, except that, the mass flow rate is very similar for both simulations.

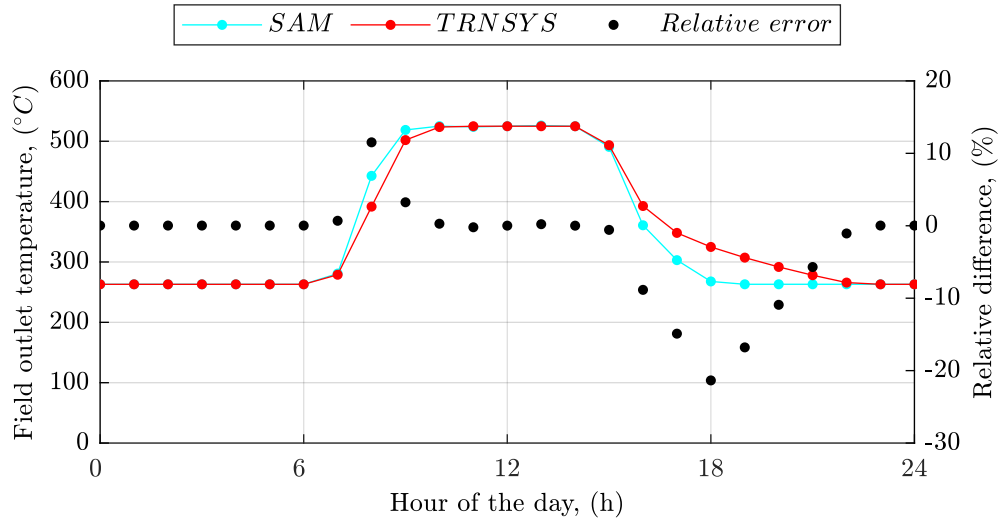

Figure 3. Solar field outlet temperature comparison, for TRNSYS© and SAM©.

Figure 3 compares the hot header temperature for the SAM© day as discussed in Figure 2. In this Figure, for which, more divergences are found, even though they seem greater, its values are small, not exceeding $\pm 20\%$. Once again, the differences are concentrated in the beginning and end of the day, moments when the control variables have a great influence on the behavior of the system. Concerning the entire system, Figure 4 shows the power through the system components.

Figure 4 shows the solar radiation profile and that, at 8 AM, the absorbed thermal energy starts to rise and, at 9 AM, there is enough energy to startup the power cycle; at 11 AM the power cycle operates at its nominal power. From 10 AM to 1 PM, the available radiation is greater than that required for the thermal cycle, with excess energy being sent to the thermal storage. After 1 PM, the solar radiation falls, and the thermal storage is discharged delivering energy to the power block to maintain its nominal power. Finally yet importantly, the annual values of the main energies in the system are compared in Figure 5.

In Figure 5 it is clear that the incident thermal power is the SAM© for both software (as expected, once the SAM©e data is used), the absorbed thermal energy for the whole year has a difference of 0.98%. When analyzing the thermal power produced and the cycle thermal input, these differences rise to 8.62% and 10.21%, respectively, which are possibly caused by different considerations in the control volumes of each software. For instance, by comparing the cycle net electrical power output, it can be observed that the difference is only 1.50%. Finally, and, in order to analyze the magnitude of the energies involved in the solar system, Figure 6 illustrates the overall energy flow.

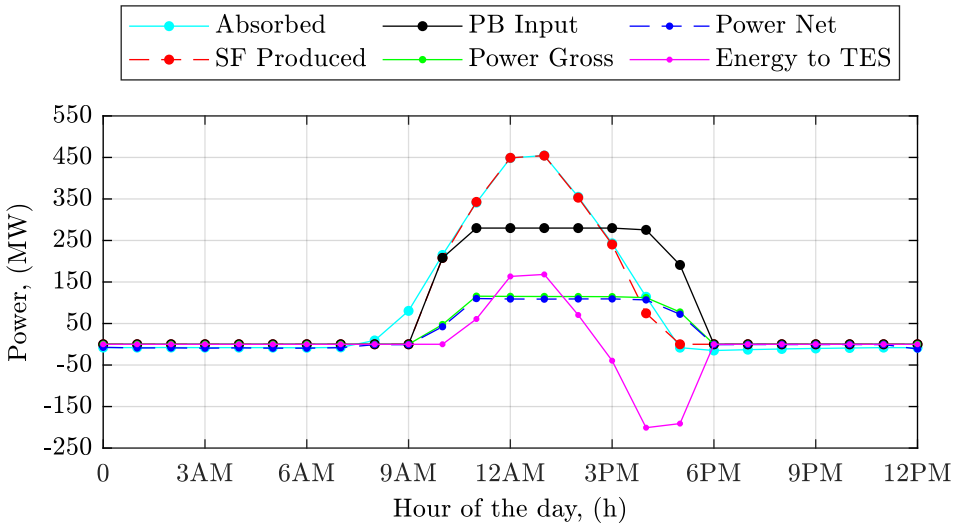

Figure 4. Power through the system components.

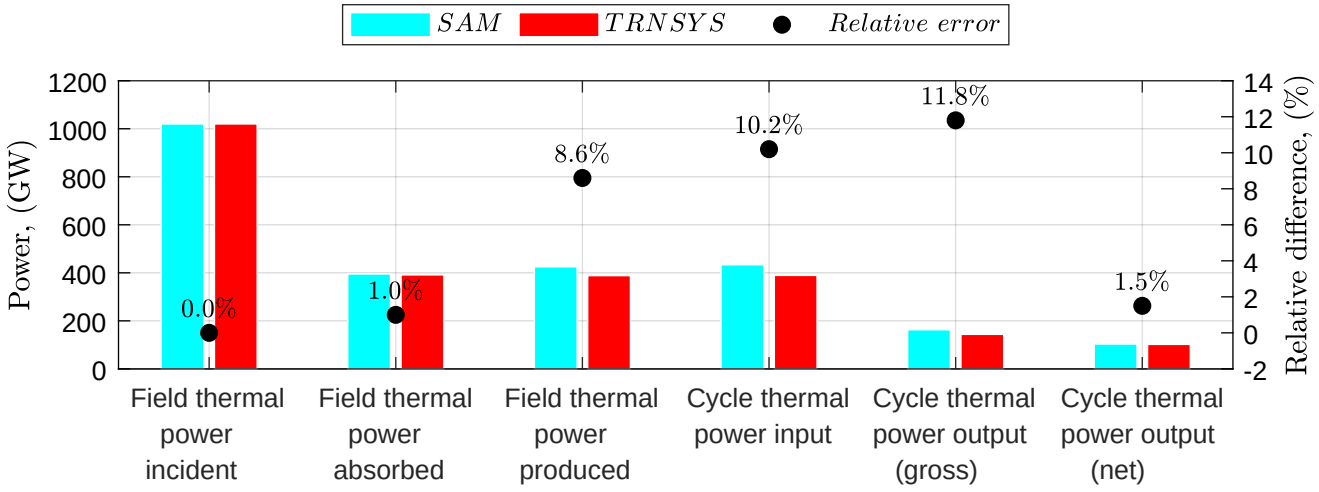

Figure 5. Comparison between TRNSYS© and SAM© in terms of annual energy flows.

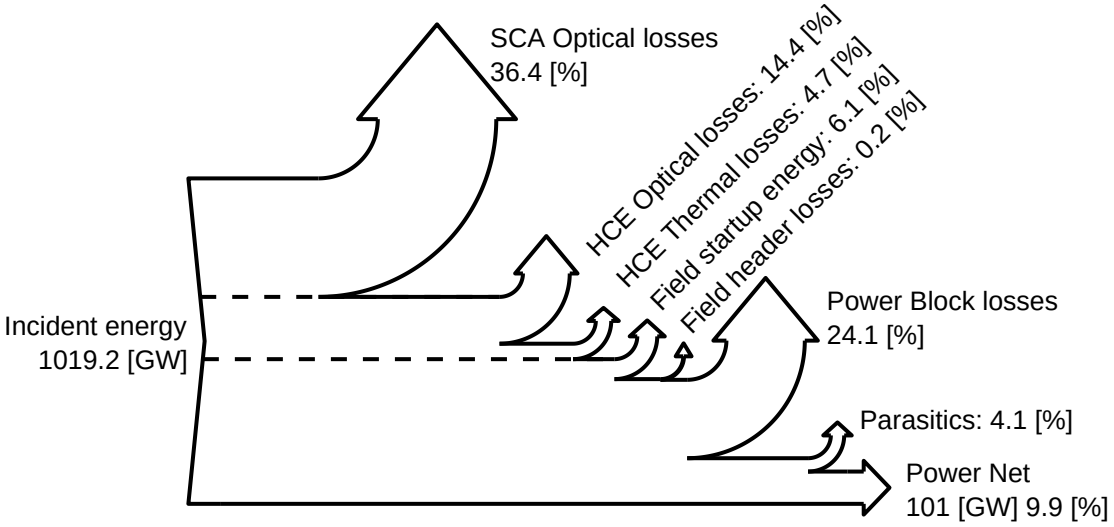

Figure 6. Sankey diagram presenting the energies and losses of the LFC-DMS solar plant.

The input of the system is the incident energy in the field, $1019.2GW$, with the first fraction related with the SCA

optical losses representing 36.4% of the incident power. The HCE optical losses correspond to 14.4% of the input energy. HCE thermal losses are 4.7%, field startup energy is 6.1% and the headers thermal losses only 0.2%. The power block losses are 24.1% and the parasitic losses 4.1%. In the end, the power net is $101GW$, or 9.9% of the incident power.

Thus, with that in mind, we found that the methodology implemented in TRNSYS© presents a behavior very similar to that of the SAM©, with some small differences regarding the strategies and control parameters, and in the control volumes. Thus, it is possible to consider that the thermal model of the collectors is correctly implemented and properly compared with the reference software.

5. CONCLUSIONS

The LFC-DMS technology shows a great potential as a renewable technology, mainly due to its capacity to use the SAM© HTF and storage media (thermal storage), constructive and operational facilities. To the best knowledge of the authors, there is not a detailed work describing the implementation of the aforementioned technology in a software for transient simulation, providing a flexible tool to address different operational schemes or optimize control strategies.

In this context, the present work aimed to present the mathematical model that best describes the behavior of the LFC-DMS system, comparing the implemented results with a reference tool, which is the System Advisor Model developed by NREL. The comparison results show very good agreement, with some differences in the end of the days, which are related to the control parameters adopted. Comparing the annual integral data, small global differences were found in the thermal absorbed energy, and in the cycle electrical energy output, where, the differences between the simulations that were found are related to the definition of control volumes used in each tool.

As an ongoing research, the present methodology presents itself as a flexible tool that can be use or further analysis, like dispatch optimization and the use of other molten salts as HTF, which, in the best knowledge of the authors, are studies that were not performed for LFC-DMS.

6. ACKNOWLEDGEMENTS

The authors would like the Brazilian National Institute of Meteorology (INMET) for providing the ground measurements. This study was financed in part by the Coordenação de Aperfeiçoamento de Pessoal de Nível Superior – Brasil (CAPES) – Finance Code 001.

7. REFERENCES

Bachelier, C. and Jäger, W., 2019. "Thermal and hydraulic evaluation of a linear Fresnel solar collector loop operated with molten salt and liquid metal". *Applied Energy*, Vol. 248, No. April, pp. 207–216. ISSN 03062619. doi:10.1016/j.apenergy.2019.04.086. URL https://doi.org/10.1016/j.apenergy.2019.04.086.

Bachelier, C. and Stieglitz, R., 2017. "Design and optimisation of linear Fresnel power plants based on the direct molten salt concept". *Solar Energy*, Vol. 152, pp. 171–192. ISSN 0038092X. doi:10.1016/j.solener.2017.01.060. URL http://dx.doi.org/10.1016/j.solener.2017.01.060.

Bellos, E., Tzivanidis, C. and Moghimi, M.A., 2019. "Reducing the optical end losses of a linear Fresnel reflector using novel techniques". *Solar Energy*, Vol. 186, No. May, pp. 247–256. ISSN 0038092X. doi:10.1016/j.solener.2019.05.020. URL https://doi.org/10.1016/j.solener.2019.05.020.

Bellos, E., Tzivanidis, C. and Papadopoulos, A., 2018. "Secondary concentrator optimization of a linear Fresnel reflector using Bezier polynomial parametrization". *Solar Energy*, Vol. 171, No. June, pp. 716–727. ISSN 0038092X. doi:10.1016/j.solener.2018.07.025. URL https://doi.org/10.1016/j.solener.2018.07.025.

Benoit, H., Spreafico, L., Gauthier, D. and Flamant, G., 2016. "Review of heat transfer fluids in tube-receivers used in concentrating solar thermal systems: Properties and heat transfer coefficients". *Renewable and Sustainable Energy Reviews*, Vol. 55, pp. 298–315. ISSN 18790690. doi:10.1016/j.rser.2015.10.059.

Colebrook, C.F., 1939. "Turbulent flow in pipes, with particular reference to the transition region between the smooth and rough pipe laws." *Journal of the Institution of Civil Engineers*, Vol. 11, No. 4, pp. 133–156. doi:10.1680/ijoti.1939.13150. URL https://doi.org/10.1680/ijoti.1939.13150.

Colla, M., Ioannou, A. and Falcone, G., 2020. "Critical review of competitiveness indicators for energy projects". *Renewable and Sustainable Energy Reviews*, Vol. 125, No. March, p. 109794. ISSN 18790690. doi:10.1016/j.rser.2020.109794. URL https://doi.org/10.1016/j.rser.2020.109794.

Forristall, R., 2003. "Heat Transfer Analysis and Modeling of a Parabolic Trough Solar Receiver Implemented in Engineering Equation Solver". , No. October, p. 164. doi:NREL/TP-550-34169.

Gallego, A.J., Sánchez, A.J., Berenguel, M. and Camacho, E.F., 2020. "Adaptive UKF-based model predictive control of a Fresnel collector field". *Journal of Process Control*, Vol. 85, pp. 76–90. ISSN 09591524. doi:10.1016/j.jprocont.2019.09.003.

Gazzo, A., Gousseland, P., Verdier, J., Kost, C., Morin, G., Engelken, M., Schrof, J., Nitz, P., Selt, J., Platzer, W. *et al.*,

2011. "Middle east and north africa region assessment of the local manufacturing potential for concentrated solar power (csp) projects".

Grena, R. and Tarquini, P., 2011. "Solar linear Fresnel collector using molten nitrates as heat transfer fluid". *Energy*, Vol. 36, No. 2, pp. 1048–1056. ISSN 03605442. doi:10.1016/j.energy.2010.12.003. URL http://dx.doi.org/10.1016/j.energy.2010.12.003.

Hakkarainen, E. and Tähtinen, M., 2016. "Dynamic modelling and simulation of linear Fresnel solar field model based on molten salt heat transfer fluid". *AIP Conference Proceedings*, Vol. 1734, No. May 2016. ISSN 15517616. doi:10.1063/1.4949161.

Hamilton, W.T., Husted, M.A., Newman, A.M., Braun, R.J. and Wagner, M.J., 2020. *Dispatch optimization of concentrating solar power with utility-scale photovoltaics*, Vol. 21. Springer US. ISBN 1108101909. doi:10.1007/s11081-019-09449-y. URL https://doi.org/10.1007/s11081-019-09449-y.

IEA, 2019. "World energy balances: An Overview". Technical Report 9. URL https://webstore.iea.org/world-energy-balances-2019.

Incropera, F.P., DeWitt, D.P., Bergman, T.L. and Lavine, A.S., 2007. *Fundamentals of Heat and Mass Transfer*. Sixth edit edition.

IRENA, 2018. *Renewable Power Generation Costs in 2018*. ISBN 978-92-9260-040-2. doi:10.1007/SpringerReference_7300. URL https://www.irena.org/-/media/Files/IRENA/Agency/Publication/2018/Jan/IRENA_2017_Power_Costs_2018.pdf.

Klein, S.A., 2010. "TRNSYS 17: A Transient System Simulation Program". *Solar Energy Laboratory, University of Wisconsin, Madison, USA*, Vol. 1, pp. 1–5. URL http://www.trnsys.com/.

OPEC, 2016. *World Oil Outlook 2016 Organization of the Petroleum Exporting Countries*. ISBN 9783950393620. URL https://www.opec.org/opec_web/static_files_project/media/downloads/publications/WOO2016.pdf.

Schneider, G., Maier, H., Stenglein, M., Schicktanz, P., Stepper, R. and Schlipf, D., 2015. "Direct Molten Salt Linear Receiver CSP-concepts with MS-TES Compared with Direct Steam Generation Linear Receiver CSP-concepts with Solid Bed TES". *Energy Procedia*, Vol. 69, pp. 1412–1420. ISSN 18766102. doi:10.1016/j.egypro.2015.03.124. URL http://dx.doi.org/10.1016/j.egypro.2015.03.124.

SPF, 2017. "SPF - Institut Für Solartechnik".

Starke, A.R., Lemos, L.F.L., Colle, S., Reinaldo, R.F., Cardemil, J.M. and Escobar, R., 2016. "A Methodology for Simulation and Assessment of Concentrated Solar Power Plants". *Revista de Engenharia Térmica*, Vol. 15, No. 1, p. 33. ISSN 1676-1790. doi:10.5380/reterm.v15i1.62162.

Tsekouras, P., Tzivanidis, C. and Antonopoulos, K., 2018. "Optical and thermal investigation of a linear Fresnel collector with trapezoidal cavity receiver". *Applied Thermal Engineering*, Vol. 135, No. February, pp. 379–388. ISSN 13594311. doi:10.1016/j.applthermaleng.2018.02.082. URL https://doi.org/10.1016/j.applthermaleng.2018.02.082.

Vasallo, M.J. and Bravo, J.M., 2016. "A MPC approach for optimal generation scheduling in CSP plants". *Applied Energy*, Vol. 165, pp. 357–370. ISSN 03062619. doi:10.1016/j.apenergy.2015.12.092.

Vouros, A., Mathioulakis, E., Papanicolaou, E. and Belessiotis, V., 2019. "On the optimal shape of secondary reflectors for linear Fresnel collectors". *Renewable Energy*, Vol. 143, pp. 1454–1464. ISSN 18790682. doi:10.1016/j.renene.2019.05.044. URL https://doi.org/10.1016/j.renene.2019.05.044.

Vouros, A., Mathioulakis, E., Papanicolaou, E. and Belessiotis, V., 2020. "Performance evaluation of a linear Fresnel collector with catoptric subsets". *Renewable Energy*, Vol. 156, pp. 68–83. ISSN 18790682. doi:10.1016/j.renene.2020.04.062. URL https://doi.org/10.1016/j.renene.2020.04.062.

Wagner, M. and Gilman, P., 2010. "Technical Manual for the SAM Physical Trough Model". *National Renewable Energy Laboratory*, , No. June.

Wagner, M.J., 2017. *Optimization of Stored Energy Dispatch for Concentrating Solar Power Systems*. Ph.D. thesis, Colorado School of Mines.

Wagner, M.J., Newman, A.M., Hamilton, W.T. and Braun, R.J., 2017. "Optimized dispatch in a first-principles concentrating solar power production model". *Applied Energy*, Vol. 203, pp. 959–971. ISSN 03062619. doi:10.1016/j.apenergy.2017.06.072. URL http://dx.doi.org/10.1016/j.apenergy.2017.06.072.

Zhu, G., Wendelin, T., Wagner, M.J. and Kutscher, C., 2014. "History, current state, and future of linear Fresnel concentrating solar collectors". *Solar Energy*, Vol. 103, pp. 639–652. ISSN 0038092X. doi:10.1016/j.solener.2013.05.021. URL http://dx.doi.org/10.1016/j.solener.2013.05.021.

Zurita, A., Mata-Torres, C., Cardemil, J.M. and Escobar, R.A., 2020. "Assessment of time resolution impact on the modeling of a hybrid CSP-PV plant: A case of study in Chile". *Solar Energy*, Vol. 202, No. April 2019, pp. 553–570. ISSN 0038092X. doi:10.1016/j.solener.2020.03.100. URL https://doi.org/10.1016/j.solener.2020.03.100.

8. RESPONSIBILITY NOTICE

The authors are solely responsible for the printed material included in this paper.